Interaction of Polyethyleneimine-Functionalized ZnO Nanoparticles with Bovine Serum Albumin

ARTICLE *in* LANGMUIR · JULY 2012

Impact Factor: 4.46 · DOI: 10.1021/la3007603 · Source: PubMed

7 AUTHORS, INCLUDING:

Soumyananda Chakraborti
Institut Curie
26 PUBLICATIONS **307** CITATIONS
SEE PROFILE

Devlina Chakravarty
Bose Institute
10 PUBLICATIONS **58** CITATIONS
SEE PROFILE

Zubaida Ansari
Jamia Millia Islamia
88 PUBLICATIONS **988** CITATIONS
SEE PROFILE

Surinder P Singh
National Physical Laboratory - India
119 PUBLICATIONS **2,261** CITATIONS
SEE PROFILE

Langmuir

Article

pubs.acs.org/Langmuir

Interaction of Polyethyleneimine-Functionalized ZnO Nanoparticles with Bovine Serum Albumin

Soumyananda Chakraborti,[†,∥] Prachi Joshi,[‡,∥] Devlina Chakravarty,[†] Virendra Shanker,[‡] Z. A. Ansari,[§] Surinder P. Singh,*[,‡,⊥] and Pinak Chakrabarti*[,†]

[†]Department of Biochemistry, Bose Institute, P-1/12 CIT Scheme VIIM, Kolkata 700054, India

[‡]National Physical Laboratory, Dr. K. S. Krishnan Marg, New Delhi 110012, India

[§]Centre for Interdisciplinary Research in Basic Sciences, Jamia Millia Islamia, New Delhi 110025, India

[⊥]Department of Engineering Science and Materials, University of Puerto Rico, Mayaguez Campus, PR 00680, United States

Supporting Information

ABSTRACT: In biological fluids, nanoparticles are always surrounded by proteins. As the protein is adsorbed on the surface, the extent of adsorption and the effect on the protein conformation and stability are dependent on the chemical nature, shape, and size of the nanoparticle (NP). We have carried out a detailed investigation on the interaction of bovine serum albumin (BSA) with polyethyleneimine-functionalized ZnO nanoparticles (ZnO-PEI). ZnO-PEI was synthesized using a wet chemical method with a core size of ∼3−7 nm (from transmission electron microscopy). The interaction of BSA with ZnO-PEI was examined using a combination of calorimetric, spectroscopic, and computational techniques. The binding was studied by ITC (isothermal titration calorimetry), and the result revealed that the complexation is enthalpy-driven, indicating the possible involvement of electrostatic interaction. To investigate the nature of the interaction and the location of the binding site, a detailed domain-wise surface electrostatic potential calculation was performed using adaptive Poisson−Boltzmann software (APBS). The result shows that the protein surface can bind the nanoparticle. On binding ZnO-PEI, the protein gets destabilized to some extent, as displayed by CD (circular dichroism) and FTIR (Fourier transform infrared) spectroscopy. Chemical and thermal denaturation of BSA, when carried out in the presence of ZnO-PEI, also indicated a small perturbation in the protein structure. A comparison of the enthalpy and entropy components of binding with those derived for the interaction of BSA with ZnO nanoparticles explains the effect of hydrophilic cationic species attached on the NP surface. The effect of the NP surface modification on the structure and stability of BSA would find useful applications in nanobiotechnology.

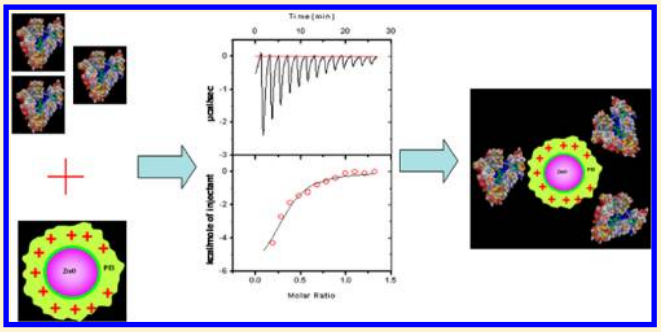

INTRODUCTION

At the interface of materials science and biology, nanoparticles provide a unique opportunity for a wide range of potential theranostic applications.[1] The advantage of nanoparticles arises from a variety of attributes, including size compatibility to biomacromolecules, high surface to volume ratio, the facile surface engineering and biomimetic functionalization, and extraordinary properties resulting from their nanometric size.[2−4] The ZnO semiconductor nanoparticles are widely applied in the technological advancements of luminescent devices,[4,5] field emitters,[6] solar cells,[7] gas sensors,[8] UV lasers,[9] etc. The intense interest in ZnO nanoparticles originates from their wide band gap, high exciton binding energy, quantum effects, biocompatibility, sensing ability, and other physico-chemical properties.[10,11] The biomedical advancements using ZnO nanoparticles (NPs) are beginning to be explored. Their preferential cancer cell toxicity, ability to generate reactive oxygen species,[12] inherent photoluminescence, etc., are getting established, making them an attractive candidate for bio-applications. ZnO adds on to the category of luminescent nanoparticles with potential utility in cell imaging and fluorescence sensing applications and has the benefit of biocompatibility over Cd-based NPs.[13] NPs are photochemically and metabolically stable and have broad excitation and a narrow and tunable emission as compared to the conventional fluorophores.[14] Water solubility of ZnO NPs, an essential feature desired for imaging, remains a key issue. There are attempts to overcome this using surface modification strategies, such as silanization, amine and polymeric coatings.[13] Blue emission of ZnO NPs in water was achieved by oleic acid and polyol capping, but its suitability is limited due to the tendency of cells and tissues to appear blue under the same UV range.[15] In this regard, polymer coatings have been found to protect yellow-green fluorescence of ZnO NPs and are more suitable in

Received: February 22, 2012
Revised: June 28, 2012
Published: July 2, 2012

biorelated labeling applications. We have earlier reported the synthesis and characterization of water-dispersed ZnO NPs with yellow-green fluorescence, prepared by using cationic polymer polyethyleneimine (PEI) to modify the ZnO surface.[16] The fluorescence was found to be centered at 555 nm under 360 nm excitation and remains stable for weeks.

PEI is well-known for its transfection ability. Among the polymer-based formulation for gene transfection, PEI is one of the most efficient polymers for nonviral gene delivery applications, and its ability to transfect a wide range of cells is well-established.[17] PEI condenses DNA and protects it from DNase degradation. Cationic PEI undergoes electrostatic complexation with negatively charged DNA, leading to the condensation of DNA and formation of polyplexes.[18] Recently, lysine−histidine-modified PEI has shown higher gene transfection efficiency of luciferase reporter gene (pRLCMV) in Neuro-2A murine neuroblastoma cells while maintaining the low toxicity.[19] Polymeric nanoparticle-conjugated PEI has exhibited high cellular uptake and reduced toxicity.[20] PEI has also been utilized for multiple bioapplications other than transfection. For example, PEI-capped Ag clusters were developed for selective and sensitive bioassay for homocysteine.[21] Apart from these applications, the polyethyleneimine nanoparticle is also attracting attention due to its inherent antimicrobial property.[22] It has been shown that the quaternary polyethyleneimine nanoparticle has long-lasting antibacterial action against the cariogenic *Streptococcus mutans*.[23] PEI capping also improves silver nanoparticle colloidal stability and the antimicrobial activity.[24]

In spite of these qualities, the toxicity of PEI always remains an issue. However, a recent study has demonstrated that the careful selection of the size of PEI polymer greatly reduces the toxicity emanating from its cationic nature. It has been shown that 10 kDa PEI was particularly efficient for allowing safe delivery of siRNA and DNA constructs with minimal or no cytotoxicity, in addition to the regular delivery of hydrophobic anticancer drug, paclitaxel, to pancreatic cancer cells.[25] According to a recent study on mutamouse FE1 cells, neither PEI polymers nor nano-ZnO crystals elicit any significant mutagenic activity or oxidative DNA damage in the exposed cells, suggesting their safe use in clinical trials.[26]

Exposure of nanoparticles to biofluids results in "corona" formation, rendering a different identity to the particles modified with serum proteins; as a result, the protein−nanoparticle interaction is a topic of particular interest.[27] Adsorption of proteins at nanoparticles' surface may result in the change of proteins' structure and activity—the extent of the change depends on both the nature of the protein as well as the surface properties of the nanoparticle.[28,29] Protein may undergo conformation change, resulting in unfolding, aggregation, the formation of the intermediate state, or the loss of activity. A recent study shows that NPs could facilitate the protein fibrillation process.[30] A number of studies revealed the nature of protein−nanoparticle interactions and the extent of protein conformation change. For example, lysozyme is found to retain its structure on adsorption to small silica and ZnO NPs,[28,31] and bovine serum albumin retains its structure and activity on binding to gold−chloroquine nanoconjugates.[32] However, the binding of ZnO NPs led to the unfolding of the periplasmic domain of ToxR protein of *Vibrio cholerae*.[33]

Serum albumins are important soluble protein constituents of the circulatory system with many physiological functions.[34] Albumins have an important role in the transport and distribution of reversibly bound various endogenous and exogenous ligands, including fatty acids, amino acids, steroids, and a variety of drugs.[35] For an administered drug, the pharmacokinetics, particularly the distribution, metabolism, and the free concentration, are strongly guided by the drug−protein interactions in the bloodstream. Therefore, for in vivo applications, it is important to understand the behavior of a nanomaterial with serum proteins. Bovine serum albumin (BSA), a heart-shaped globular protein, presents an ideal model of serum carrier protein. BSA has 76% sequence identity with human serum albumin (HSA) and has two fluorophores as compared to one fluorophore in the latter.[36] The tryptophan fluoresence in BSA provides a convenient mode for detecting structural changes that occur upon nanoparticle binding. Serum albumins have an important role in cellular uptake and internalization. There are reports on enhanced cellular uptake, particularly of nanoparticles in the presence of albumins.[37] Nonspecific adsorption of serum proteins mediates the uptake of the nanoparticles via nonspecific or receptor-mediated endocytosis and dictates their fate in the intracellular environment.[38] There are reports that PEI-mediated transfection increases in the presence of serum.[17] Elaborated studies showed that serum albumins enhance the polyethylenimine-mediated gene delivery and cell transfection in a wide variety of cultured cells, not only at the transfection level but also at the total percentage of transfected cells.[39]

The escalating application of PEI-capped nanoparticles in different domains of nanomedicine has led us to investigate the mechanism of interaction between the ZnO-PEI nanoparticle (ZnO-PEI, in short) and BSA. To be useful in bioapplications, ZnO-PEI should not have any adverse effect on the structure and activity of BSA. Also, the binding of NPs with BSA should be moderate enough to enable a sustained release of ZnO-PEI at the appropriate site. We observed enthalpy-driven binding involving electrostatic interactions, and the thermodynamic parameters have been compared to those observed for the uncapped ZnO NPs. The protein retains its native structure on binding to ZnO-PEI, with only minor alterations in the secondary and tertiary structures. Chemical and thermal denaturation studies also support this finding. We believe that the present study will provide useful insight into protein−nanoparticle interaction, consolidating our understanding of biodistribution and biomolecular recognition of functionalized nanoparticles.

MATERIALS AND METHODS

Materials. Zinc acetate dihydrate ($Zn(Ac)_2{\cdot}H_2O$), ≥99.0%), lithium hydroxide monohydrate ($LiOH{\cdot}H_2O$, ≥99.0%), anhydrous ethanol (98%), trisodium citrate dehydrate (≥99%), and polyethyleneimine (branched, MW 10 kDa) were purchased from Sigma-Aldrich and used as is. Bovine serum albumin (BSA) was purchased from Sigma and used without further purification. All other reagents were of analytical grade, and double-distilled water was used throughout the experiment. Phosphate buffer of 0.1 mM concentration was used for protein solutions.

Synthesis of ZnO-PEI. The ZnO NPs were prepared by modified sol−gel route and subsequently treated by trisodium citrate followed by polyethyleneimine (PEI). The detailed synthesis process is described elsewhere.[16]

Sample Preparation for ZnO-PEI-Conjugated BSA. BSA protein solution (concentration 5 μM) was exhaustively dialyzed using a dialysis membrane (Spectra Biotech membrane MWCO: 3500, Spectrum Lab, CA, USA) against buffer solution at 4 °C. A buffer solution, consisting of 0.1 mM of sodium phosphate at pH 7.4, was used in all of the experiments. To study the interaction between ZnO-

PEI and BSA, a fixed amount of the NP was added to the protein solution, mixed by vortexing and incubated at room temperature for 2 h.

Optical Spectroscopy. The formation of ZnO-PEI was verified by determining optical absorption from UV−vis absorption spectroscopy. The band gap absorption of ZnO appears in the UV region, and the corresponding Tauc plot provides the band gap of prepared ZnO-PEI. The optical absorption spectrum was recorded using an Ocean-Optics HR4000 spectrometer equipped with a Toshiba TCD1304AP linear CCD array detector that enables optical resolution as precise as 0.02 nm (FWHM). The optical response is taken from 300 to 400 nm range in a 10 mm path quartz cuvette.

FTIR Spectroscopy. FTIR technique was used to determine the binding of PEI to ZnO. FTIR scanning was performed with constant nitrogen purging using a Perkin-Elmer spectrometer equipped with a DTGS KBr detector and a KBr beam splitter with constant nitrogen purging. IR grade KBr was used as scanning matrix. Then, 1−2 mg of fine sample powder and 90−100 mg of KBr powder were mixed and dried completely, then transferred to 13 mm dye to make a nearly transparent and homogeneous pellet. All spectra were taken at 4 cm^{-1} resolution, averaged over 20 scans in the range of 400 to 4000 cm^{-1}. To characterize ZnO-PEI-BSA conjugates, these were washed with D_2O three times and suspended in a minimum volume of D_2O. Samples were diluted 20 times before the measurement. The final spectra were collected after subtracting the background spectra of D_2O. All spectra were taken in the range from 1450 to 1750 cm^{-1} particularly for the characterization of the amide bond in protein.

Electron Microscopy. The particle size and dispersity of the prepared nanoparticles were studied using transmission electron microscopy (TEM). TEM grids were prepared by placing 10 μL of the diluted and well-sonicated sample solutions on a carbon-coated copper grid and dried completely in dust-free atmosphere. The bright-field electron micrographs of the samples had been recorded on a JEM-2010 (device: Orius SC1000) at the accelerating voltage of 200 kV.

Atomic Force Microscopy. To determine the morphology of PEI-functionalized ZnO NPs on a silicon wafer surface, deposited by spin-casting, the samples were analyzed ex situ by atomic force microscopy (AFM). AFM characterization was carried out using a Digital Instruments Nanoscope III. AFM measurements were performed in tapping mode using a Si_3N_4 tip with a resonance frequency of 100 kHz and a spring constant of 0.6 N m^{-1} to obtain the surface topography of deposited ZnO-PEI NPs. The film was air-dried in a dust-free environment before taking measurement.

Isothermal Titration Calorimetry (ITC). Isothermal titration calorimetry measurement was performed on a VP-ITC calorimeter (Microcal Inc., Northampton, MA). BSA was dialyzed extensively against 0.1 mM sodium phosphate buffer, and ZnO-PEI was dissolved in the same dialysate. A typical titration involved 13 injections of the protein (the titrant) (20 μL aliquot per injection from a 1 mM stock solution) at 5 min intervals into the sample cell (volume 1.4359 mL) containing ZnO-PEI (concentration, 150 μM) (BSA/ZnO-PEI ratio was 7:1, instead of usual 10:1, to avoid the effect of loading excess protein).[40,41] The titration cell was stirred continuously at 310 rpm. The heat of the ligand dilution in the buffer alone was subtracted from the titration data for each experiment. The data were analyzed to determine the binding stoichiometry (N), affinity constant (K_a), and other thermodynamic parameters of the reaction using curve fitting analysis.[42] The titration of protein with ZnO-PEI was carried out at 25 °C. The reported values are the average of two parallel experiments. For studying the interaction of the uncapped ZnO with BSA, the former was used as the titrant, with the nanoparticle and protein concentrations being 1 mM and 150 μM, respectively.

Fluorescence Spectroscopy. Fluorescence spectroscopy was used to determine the change in tryptophan fluorescence on binding of BSA to ZnO-PEI. All of the fluorescence measurements were carried out using a Hitachi F3000 spectrofluorimeter with 2 μM protein. The following three sets of measurements were performed.

(i). Trp Fluorescence Quenching. To determine the Trp fluorescence quenching, the ZnO-PEI was added to the protein from a 0.1 mM stock solution. The excitation wavelength was set at 295 nm to selectively excite tryptophan residues, and the emission was monitored in the range of 310−400 nm with the fixed slit width of 5 nm. The fluorescence intensities were determined at the λ_{max}, and after inner filter correction, the data analysis was done using the Stern−Volmer equation.[43]

$$F_o/F_c = 1 + K_{SV} \times [\text{ZnO-PEI}] = 1 + K_q\tau_0[\text{ZnO-PEI}] \quad (1)$$

where F_o and F_c denote the steady-state fluorescence intensities in the absence and presence of the quencher (ZnO-PEI), respectively; K_{SV} is the Stern−Volmer quenching constant, and [ZnO-PEI] is the concentration of the quencher. K_q is the bimolecular quenching constant, and τ_0 is the lifetime of the fluorophore. For the protein ligand association reaction, the following equation was employed for the calculation of the binding constant representing the static quenching

$$\log(F_o - F_c)/F_c = \log K_b + n \log[\text{ZnO-PEI}] \quad (2)$$

where K_b is the binding constant and n is the number of binding sites.

(ii). Chemical Denaturation Study. Unfolding of the native and the NP-conjugated proteins in the presence of increasing concentration of GdnHCl was monitored by studying the change in tryptophan fluorescence (λ_{max}) and expressed as the fraction of the unfolded protein against GdnHCl concentration. To determine the free energy of unfolding, data were fitted in a standard two state protein unfolding equation.[44]

(iii). Fluorescence lifetime Measurement. Fluorescence lifetime of BSA was calculated using a time-correlated single-photon counter from Edinburgh Instrument, UK. The decays were recorded at an excitation of 295 and an emission of 342 nm and using an emission polarizer at a magic angle of 54.7°. Decay curves were fitted using the following equation

$$G(t) = \sum_i B_i \exp(-t/\tau_i) \quad (3)$$

where $G(t)$ is the fitted decay curve of the sum of all exponential terms and B_i is the pre-exponential factor for the ith component. The biexponential nature of the fluorescence decay was judged from the reduced χ^2 values (1−1.2).

Circular Dichroism (CD) Spectropolarimetry. To determine the proteins secondary structure, CD spectra were obtained using a JASCO-810 spectropolarimeter equipped Peltier-type temperature controller and a thermostatically controlled cell holder. The temperature of the sample was controlled at 25 ± 0.1 °C. A 1 mm path length cuvette was used for measurements. For all of the measurements, a protein concentration of 5 μM was used. The far-UV region was scanned between 200 and 260 nm with an average of three scans and a bandwidth of 5 nm. The final spectra were obtained by subtracting the buffer contribution from the original protein spectra. The CD results were expressed in terms of mean residual ellipticity (MRE) in deg·cm^2·$dmol^{-1}$ defined as

$$[\theta] = [\theta]_{obs}/10nlc_p \quad (4)$$

where $[\theta]_{obs}$ is the observed ellipticity in degrees, c_p is the protein concentration in mol/L, n is the number of residues in BSA, and l is the path length of the cell (path of light) in cm. The CD spectrum of buffer was subtracted as the baseline.

For determining the melting temperature of protein in the presence and absence of ZnO-PEI, the temperature-dependent CD was performed in the temperature range of 25−90 °C at the rate of 30 °C h^{-1}. For near-UV CD measurement, the spectra were recorded in the range of 260−320 nm wavelengths using a protein concentration of 50 μM and 0.5 cm path length quartz cuvette. All of the data provided here are averages of three identical measurements.

Esterase Activity. Esterase activity of BSA was determined with the synthetic substrate p-nitrophenyl acetate by following the formation of p-nitrophenol at 400 nm, using a Shimadzu 2401 spectrophotometer.[45] The reaction mixtures contained 50 μM p-nitrophenyl acetate and 20 μM protein in 50 μM phosphate buffers,

dx.doi.org/10.1021/la3007603 | Langmuir 2012, 28, 11142−11152

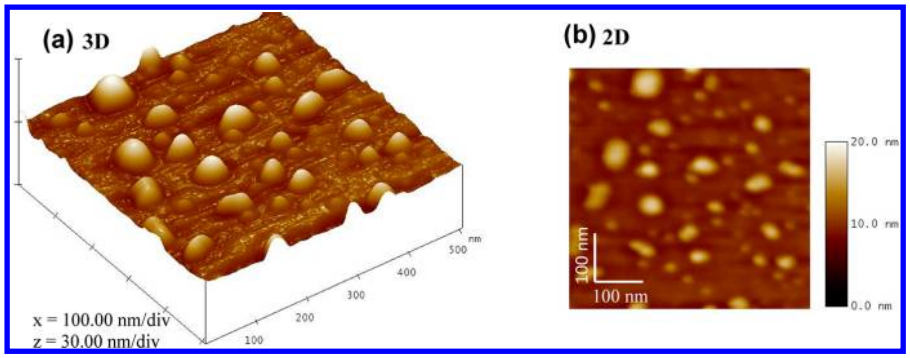

Figure 1. AFM of PEI-functionalized ZnO NPs (a) in 3D with *x,y* axis scale = 100 nm/div and *z* axis scale = 30 nm/div and (b) in 2D with AFM height 20 nm in *z* axis and *x,y* scale bar = 100 nm.

pH 7.4 at 37 °C. A molar extinction coefficient [ε = 17 700 M^{-1} cm^{-1}] for *p*-nitrophenol was used for all of the calculations. One unit of esterase activity was defined as the amount of enzyme required to liberate 1 μM of *p*-nitrophenol per minute at 37 °C.

Structural Analysis. Modeling of BSA was performed using the same protocol stated earlier.[32] PDB2PQR (version 1.7.1) (http://kryptonite.nbcr.net/pdb2pqr/) was used to calculate the charges on the protein at physiological pH.[46,47] The software employs a continuum electrostatics method along with Amber force field. Accessible surface area was calculated using the program NACCESS (http://www.bioinf.manchester.ac.uk/naccess). The surface residues were identified as those having relative surface accessibility ≥5%; from these, the acidic (total charge on residue ≤−0.001) and basic residues (total charge on residue ≥0.001) were identified. Adaptive Poisson−Boltzmann solver (APBS) was employed to study the electrostatic properties of the protein surface.[48] APBS solves the Poisson−Boltzmann equation (PBE) to describe the surface potential of the protein. Charges on protein, as generated using PDB2PQR, were given as input to APBS. Details about the software and the examples of what one can do with it can be obtained from http://www.poissonboltzmann.org/apbs. Pymol (http://www.pymol.org) was used for visualization. Electrostatic potential calculated using eF-site (http://ef-site.hgc.jp/eF-site/index.jsp) gave a similar result.

RESULTS

Physicochemical Properties of ZnO-PEI. ZnO-PEI was synthesized as reported.[16] Figure S1 (Supporting Information) gives the schematic representation of the synthesis. The sol−gel-derived ZnO NPs were treated with trisodium citrate, a linker for efficient PEI binding. Trisodium-citrate-capped ZnO NPs were brought in contact with aqueous solution of PEI, resulting in PEI-functionalized ZnO NPs. The ZnO-PEI was found to have bright yellow-green fluorescence centered on 555 nm using 360 nm excitation. The solution was found to be stable for weeks while retaining its fluorescence properties. The physicochemical characteristics are discussed below. The preparation and characterization of ZnO NPs were as described.[31]

Optical Properties and Binding Characteristics. Figure S2a illustrates the Tauc plot of water-dispersed ZnO-PEI corresponding to its optical absorbance spectra shown in the inset. The plot was constructed between $(\alpha h\upsilon)^2$ and $h\upsilon$ (eV) for the direct band gap semiconductor ZnO. The optical absorbance shows that ZnO-PEI absorbs in a wide range of energy with a maximum at 345 nm. The Tauc plot revealed the band gap of ZnO-PEI NPs as 3.62 eV, higher than the bulk band gap of 3.3 eV for ZnO, suggesting the effect of quantum confinement on ZnO-PEI due to their small size.

The FTIR spectrum of ZnO-PEI, shown in Figure S2b, indicates the typical metal oxide (Zn−O) peak at 465 cm^{-1}, suggesting the formation of ZnO material. The ZnO-PEI shows strong twin peaks at 1587 and 1388 cm^{-1} and a broad peak in the 3200−3400 cm^{-1} region. The strong signature at 1587 cm^{-1} is assigned to the N−H bending mode of the amine group overlapped with the C−H bending mode of the methylene ($-CH_2$) group. The peak at 1388 cm^{-1} is due to the C−H bending vibration of the methyl ($-CH_3$) group. The symmetric and asymmetric stretching modes of N−H appear at higher frequency located around 3389 and 3250 cm^{-1}. The peaks in the 2830−3000 cm^{-1} region are attributed to the symmetric and asymmetric C−H stretching modes of the $-CH_2$ and $-CH_3$ groups. The C−N stretch appears in the 1000−1250 cm^{-1} region; the peak at 645 cm^{-1} is attributed to the open long chain $(-CH_2)_n$ bending. The amide bond linking the citrate to PEI generally comes in the near region of 1600 cm^{-1}. In the present spectrum, it appears to be overlapped with the N−H bending mode as the number of amines is comparatively higher in the compound.

Particle Size and Structure. Figure S3a shows the electron diffraction pattern of ZnO-PEI NPs. The bright diffraction rings present in the pattern correspond to the various crystal planes of ZnO. The rings corresponding to (101), (002), and (100) planes are found to be intense compared to the other (102), (110), (103), and (112) planes, suggesting the hexagonal wurtzite structure of ZnO NPs; the diffraction ring corresponding to the (002) plane appears to get merged with the ring corresponding to the plane (101) attributed to the nanometric size of particles. Figure S3b shows the TEM micrograph of water-dispersed ZnO-PEI NPs at 20 nm scale, and the average range of particle size distribution is 3−7 nm, indicating the NP core. Figure S3c gives the high-resolution TEM micrograph at 2 nm scale displaying the lattice spacing of 0.278 nm.

Surface Morphology Using AFM. High-resolution AFM images of ZnO-PEI NPs showing the surface morphology are shown in Figure 1. Usually, the surface morphology studies do not provide the individual particle size; rather they show the average grain size at the deposited film surface. It can be seen that the spin-casted ZnO-PEI exhibits size dispersity containing both large and smaller grains. The smaller grain size covers the range of 10−15 nm, while the larger grain size is in the 45−65 nm range, though the average height of grains is nearly 20 nm. The surface morphology measurements suggest that the spin-casting increases the grain size of ZnO-PEI at the silicon surface as compared to the dispersed small particles in solution. The mole ratio of ZnO and PEI in the capped NP is found to be 1:0.053 (Supporting Information Table S1).

dx.doi.org/10.1021/la3007603 | *Langmuir* 2012, 28, 11142−11152

Binding of BSA to ZnO-PEI. *Thermodynamics of Binding.* ITC has been employed to measure the binding thermodynamics and stoichiometry between ZnO-PEI and BSA in solution. The thermogram for BSA and ZnO-PEI titration is shown in Figure 2, and the derived parameters are shown in

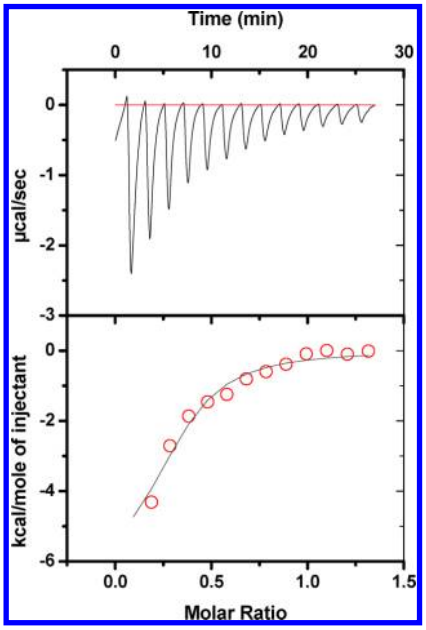

Figure 2. ITC data from the titration of BSA with ZnO-PEI. Heat flow versus time during injection of BSA over ZnO-PEI at 25 °C and heat evolved per mol of added BSA against the molar ratio (BSA to ZnO-PEI) for each injection, shown at top and bottom, respectively. The data were fitted to a standard model.

Table 1. ITC-Derived Thermodynamic Parameters for the Binding of BSA to ZnO-PEI and ZnO NP at 25 °C[a]

parameter	ZnO-PEI	ZnO NP
K_a (binding constant, M^{-1})	7.94 (±3) × 10^4	2.6 (±0.6) × 10^4
N (stoichiometry, protein:NP)	0.3 (±0.06)	1 (±0.11)
ΔH (binding enthalpy, kcal/mol)	−6.4 (±1.6)	−4.3 (±0.7)
ΔS (entropy change, cal/mol·K)	0.75	6
$-T\Delta S$ (kcal/mol)	−0.22	−1.8
ΔG (free energy change, kcal/mol)	−6.6	−6.1

[a]Based on Figures 2 and S5.

Table 1. The interaction of ZnO-PEI with BSA is found to be enthalpically favored (i.e., $\Delta H < 0$). The contribution of entropy is negligible compared to that from enthalpy. The negative value of enthalpy is directly related to weak van der Waals interactions and/or electrostatic interactions during the protein−NP complex formation.[49] The stoichiometry (BSA to NP) is found to be 0.3, which means that each nanoparticle is surrounded by at least three protein molecules. The binding constant on the order 4 indicates moderate binding between the two components, and the value is comparable with the result from fluorescence studies (following section).

Intrinsic Tryptophan Fluorescence Quenching. BSA has two Trp residues at positions 134 and 212. Trp212 residue is located in the largest hydrophobic cavity of the protein known as Sudlow's site I, whereas Trp134 is located on the surface of the subdomain Ib. If the binding occurs in any of these domains close to Trp, tryptophan fluorescence quenching can be observed. Therefore, the intrinsic fluorescence quenching of Trp is used to determine the proximity of the Trp residue to the NP in the BSA−NP complex. Adsorption of protein on the ZnO-PEI surface results in the decrease in the maximum fluorescence intensity (Figure 3)—the fluorescence intensity decreases progressively with increasing NP concentration. The question is which Trp gets quenched on NP binding. The answer lies in the relative position of the Trp residues as well as the nature of the interaction. If NP binds near Trp212, the interaction must be hydrophobic in nature; but our ITC data clearly indicate that the binding is more of electrostatic in nature. As Trp212 lies in a hydrophobic cavity, the binding must occur in close vicinity of Trp134. A fluorescence quenching study had earlier indicated that PEI by itself binds to the same region.[50]

The binding between BSA and ZnO-PEI was further investigated using the Stern−Volmer equation (eq 1).[43] The plot (Figure 3b) provides a value of 4 × 10^4 M^{-1} for the constant K_{SV}. Using the τ_0 value 10^{-8} s, the quenching rate constant K_q for the complexation is calculated to be 4 × 10^{12} M^{-1} s^{-1} (using eq 1). The quenching of Trp may be induced due to a collision process and/or the formation of a complex with the quencher. The maximum scattering quenching constant for various kinds of quenchers to protein is reported to be 2 × 10^{10} M^{-1} s^{-1}.[42] The experimentally determined value of K_q is greater than that of the scattering quenching, indicating that the quenching is static in nature (not dynamic), which is also inferred from the average lifetime of BSA (discussed later). The straight line obtained in the Stern−Volmer plot is also indicative of the existence of a single type of quenching mechanism. Further, eq 2 is used to determine the binding constant (K_b) from the quenching experiment, and based on the plot (Figure 3c), the value is found to be 6.4 × 10^4 M^{-1}. Although the protein:NP stoichiometry from Figure 3bc is indicated to be 1, such values derived from fluorescene quenching data may sometimes be misleading,[51] and the value given by ITC is more reliable.

Structure of BSA on Binding to ZnO-PEI NPs. CD is a very powerful and sensitive technique for evaluating conformational changes in protein on binding to nanoparticle.[52] The far-UV CD spectrum has been used to determine the change in the secondary structure of BSA on interaction with ZnO-PEI (Figure 4a). BSA, mostly an α-helical protein, produces very strong negative signals at 208 and 222 nm, characteristics of α-helical structure, and any variation in these bands will indicate conformational change in the native structure.[53] On addition of ZnO-PEI to BSA, the negative ellipticity values decrease slightly, suggesting minor loss of helical contents. (That the decrease in signal was not due to any possible loss of solubility of the protein was ascertained by checking the OD of the protein before and after the addition of NP—there was no change in the value.) The shape of the peaks and their positions remain unaltered, indicating that the protein manages to retain its overall structure. Near-UV CD gives information about the tertiary structure of protein. Phe (262−267 nm) along with Tyr and Trp (282−290 nm) produces strong signals in this region. Any change in the signal intensity implies a structural change in protein. We have found very little alterations in the ellipticity values on binding to NP (Figure 4b), suggesting only a minor change in the three-dimensional configuration of the protein.

As any free protein (not bound to ZnO-PEI) present would affect the CD signal, we checked the OD of the supernatant

dx.doi.org/10.1021/la3007603 | *Langmuir* 2012, 28, 11142−11152

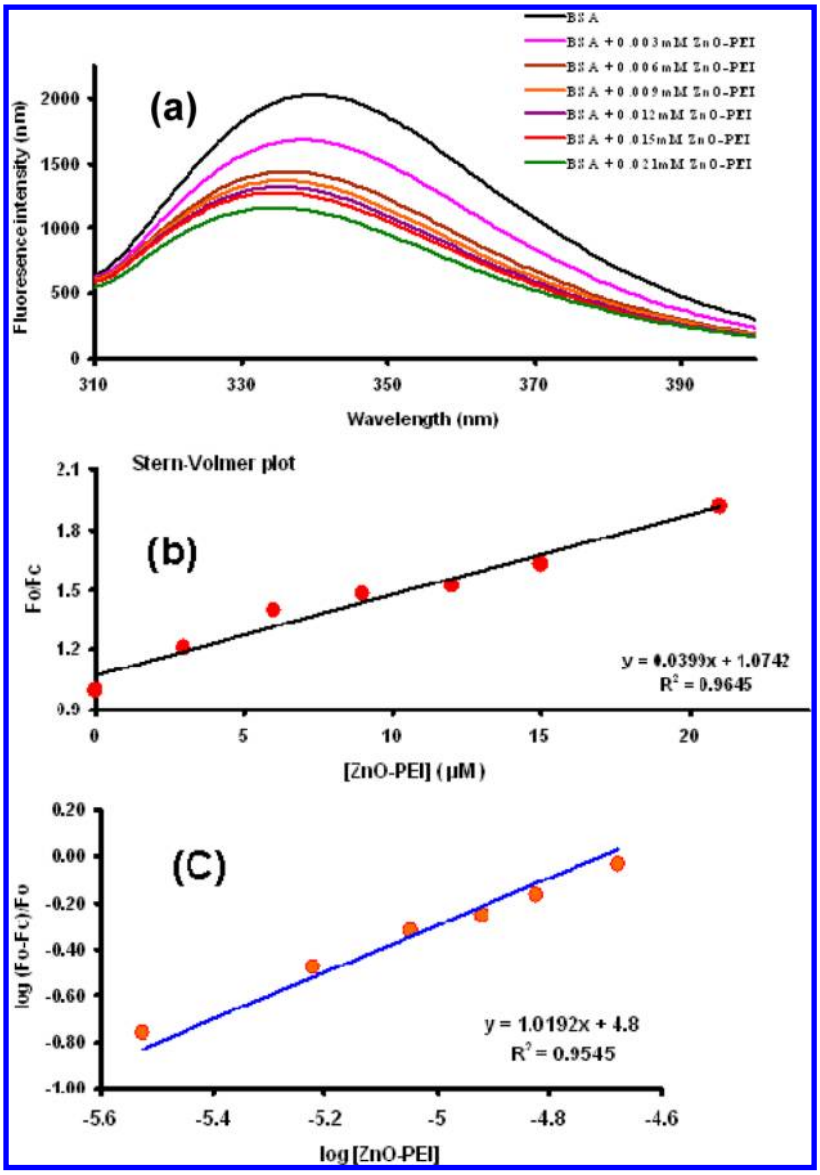

Figure 3. Tryptophan fluorescence of BSA on binding to ZnO-PEI. (a) Quenching of tryptophan (Trp212) fluorescence by varying concentrations of ZnO-PEI. (b) Stern−Volmer plot derived from the quenching data. The equation of the fitted line is $F_o/F_c = 1.0742 + 0.0399 \times [\text{ZnO-PEI}]$ ($R^2 = 0.9645$). (c) Plot of $\log[(F_o - F_c)/F_c]$ vs $\log[\text{ZnO-PEI}]$ for the BSA-ZnO-PEI system, and the equation used for the fitted line is $\log[(F_o - F_c)/F_c] = 1.019 \log[\text{ZnO-PEI}] + 4.8$ ($R^2 = 0.95$).

after spinning the sample at 14 000 rpm for 15 min;[54] a negligible value indicated that BSA was present and bound to ZnO-PEI only. We also checked the effect of increasing the concentration of ZnO-PEI on the CD spectra (Figure S4) and the derived secondary structure content (Table S2). Beyond the BSA/ZnO-PEI ratio of 1:2 (for which the data are presented in Figure 4), there is only marginal decrease in helical content. The decrease seems to be much lower than what has been observed for lysozyme or β-lactalbumin adsorbed on silica NPs, where a higher NP concentration and the corresponding smaller protein surface concentration led to the unfolding of the protein to a greater extent in the equilibrium state.[55,56]

The effect on secondary structure of BSA is further confirmed by FTIR spectroscopy (Figure 4c). The amide I and amide II bands of protein reveal the information on the proteins' conformation change. The amide I band due to C═O stretch, appearing in 1600−1700 cm^{-1} region, is corelated to proteins' secondary structure, whereas the amide II band due to coupling of C−N stretch and N−H bending modes appears in the 1500−1600 cm^{-1} region, indicating the adsorption of protein at solid surfaces. In the amide I band, the region of 1652−1662 cm^{-1} is contributed by α-helix.[31] The peak around 1658 cm^{-1} observed for free BSA is attributed to the helical content of protein structure. On binding to ZnO-PEI, the peak appeared around 1656.6 cm^{-1} with decreased intensity, indicating some loss of the helical structure, corroborating the results from the far-UV CD measurements. The amide II peak for native BSA emerges around 1541 cm^{-1} in spectrum, which gets shifted to 1537 cm^{-1} in ZnO-PEI-bound BSA, suggesting the adsorption of the protein at the NP surface. On the basis of the above investigation, it can be stated that, on NP binding, the protein retains its essential structural features. However, the changes in the CD and FTIR signals can be attributed to the local conformational changes in the binding pocket of the protein due to the interaction.

dx.doi.org/10.1021/la3007603 | *Langmuir* 2012, 28, 11142−11152

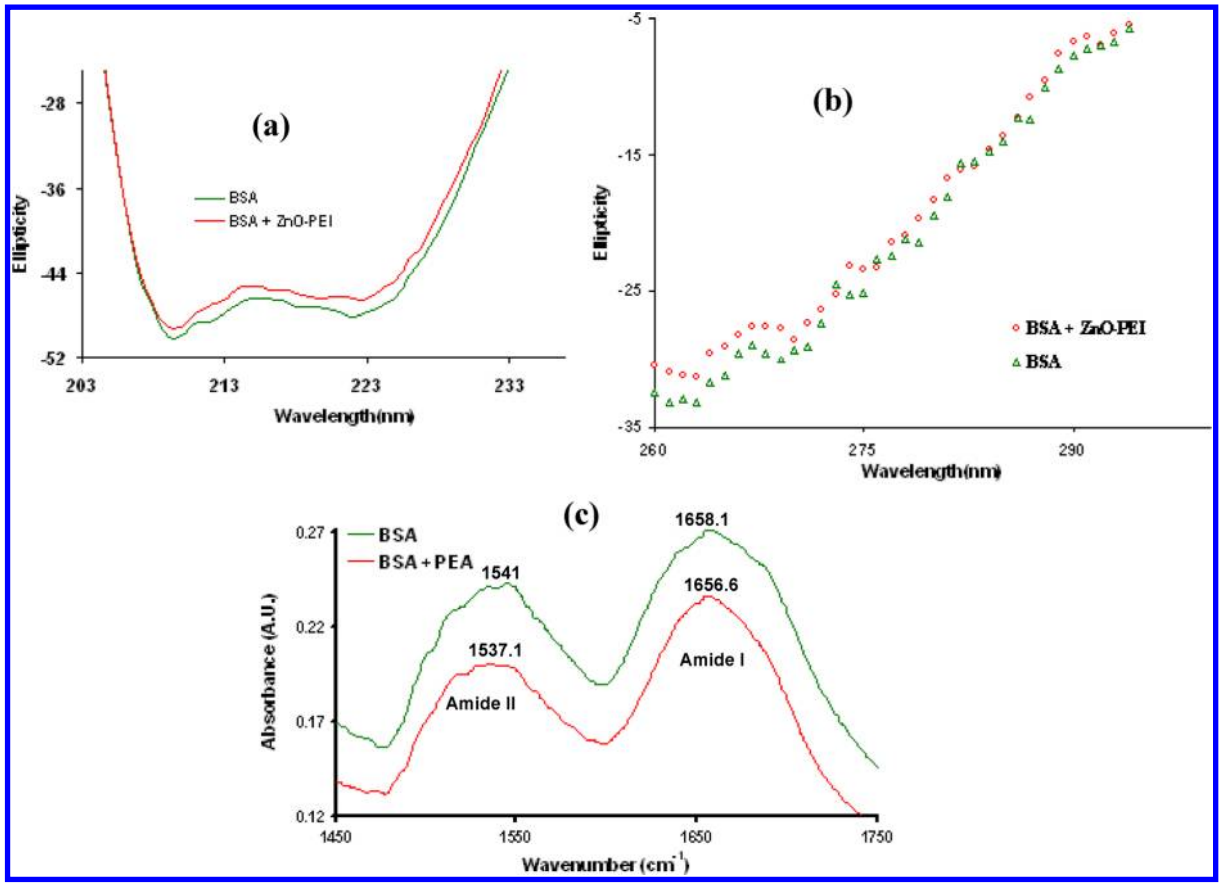

Figure 4. Characteristic spectra of BSA in the absence and presence of ZnO-PEI. (a) Far-UV CD spectra, (b) near-UV CD spectra, and (c) FTIR spectra.

Table 2. Fluorescence Lifetime of BSA in the Presence and Absence of ZnO-PEI

	fluorescence lifetime component				relative abundance of lifetime component		statistical deviation	average lifetime
sample	τ_1 (ns)	std. dev.	τ_2 (ns)	std. dev.	τ_1 (%)	τ_2 (%)	χ^2	τ (ns)
BSA	3.05	0.13	6.84	0.05	15.7	84.35	1.1	6.25
BSA + ZnO-PEI	3.7	0.17	7.04	0.65	21.1	78.9	1.18	6.34

Time-Resolved Fluorescence Decay. The fluorescence characteristics, such as the average fluorescence lifetime and the components of lifetime of protein fluorophore tryptophan, are sensitive to the environment and hence indicative of the protein conformational alterations during protein−ligand interactions.[57] Therefore, time-resolved fluorescence lifetime is considered to be an important tool to detect conformational changes in protein on binding to other molecules, as the conformational change significantly affects the population distribution among the exited states of the emitting fluorophore Trp.[58] The fluorescence decay of BSA shows a biexponential decay curve of the average life of 6.25 ns (Table 2). The lifetime components are found to be 3.05 and 6.84 ns with relative abundance of 15.7 and 84.35%, respectively. For ZnO-PEI-bound BSA, the fluorescence decay curve remains biexponential with an average life of 6.34 ns, quite close to that of free BSA. The lifetime components also remain close to that of BSA and are found to be 3.7 and 7.04 ns with the relative abundance of 21.1 and 78.9%, respectively. There is no significant change observed in the average lifetime, lifetime components, and their percent abundance, suggesting that the binding of ZnO-PEI has no adverse affect on protein structure. Only some small perturbations could be inferred from CD, FTIR, and fluorescence decay measurements.

Chemical and Thermal Denaturation of BSA in the Presence ZnO-PEI. The effect of NP conjugation on the BSA denaturation was investigated using Trp fluorescence. First, 6 M GdnHCl was used to completely denature the protein. It was observed that the unfolding of BSA started at 1.5 M and was complete at 3.5 M GdnHCl concentration with a midpoint occurring at 2.5 M (Figure 5). These values of the start and the end points of transitions are independent of the presence or absence of NP. Finally, the data were fitted to a two-state protein unfolding model to obtain the unfolding free energy (ΔG_{NU}),[44] which indicated that ZnO-PEI destabilizes the folded form of BSA by 0.4 kcal/mol (Table 3). Normally, m_{NU} is related to the difference in solvent-accessible surface areas (ΔASA) between the unfolded and the native states. As expected, the m_{NU} value of BSA is also lowered by ~0.2 kcal/mol/M on binding to NP. We also measured the thermal unfolding of BSA in the presence and absence of ZnO-PEI. The data show a gradual reduction in ellipticity value with increasing temperature for both native and bound BSA, suggesting loss in helical content as a result of temperature-induced protein

dx.doi.org/10.1021/la3007603 | *Langmuir* 2012, 28, 11142−11152

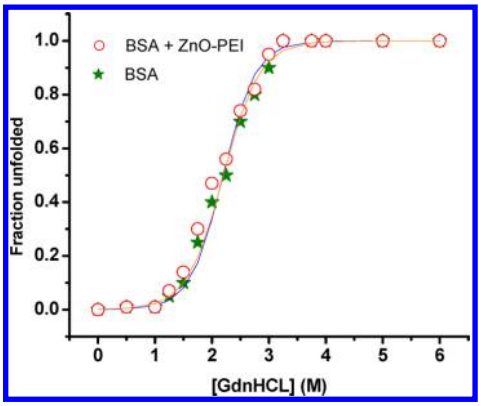

Figure 5. Chemical denaturation of BSA and ZnO-PEI-bound BSA in the presence of increasing concentration of GdnHCl. Data were fitted to a standard two-state model.

Table 3. Parameters Representing GdnHCl-Induced Unfolding of BSA in the Presence and Absence of ZnO-PEI[a]

	in the absence	in the presence
ΔG_{NU} (kcal/mol)	4.64 (±0.4)	4.2 (±0.4)
m_{NU} (kcal/mol/M)	2.1 (±0.2)	1.9 (±0.2)

[a]Values obtained by fitting to a standard two-state equation of unfolding.

unfolding. In all of our analysis, the thermal unfolding can be evaluated by using only two basis spectra: the "folded" starting spectrum consists of all α-helical structure, and the "unfolded" spectrum contains random structure. The increase of the unfolded state of protein with temperature has been fitted with a sigmoid curve for a simple two-state unfolding transition; the analysis resulted in a melting temperature (T_m) of 65 °C for BSA, which is reduced by ~5 °C on NP conjugation (T_m = 60 °C) (Figure 6). The result indicates that NP binding leads to some perturbation in the protein structure due to which the thermal stability of the protein gets somewhat decreased.

DISCUSSION

Due to unique physicochemical properties, ZnO nanomaterial has various bioapplications.[10] The introduction of nanoparticles in the biological fluid is associated with interaction with plasma proteins, especially albumin. Albumin also plays a crucial role in receptor-mediated endocytosis, leading to internalization of nanoparticles. Although there are reports on ZnO-BSA interaction, ZnO suffers from the drawback of the formation of uncontrollable aggregates at physiological pH. The aggregate causes nonspecific adsorption of protein and the reduction of the effective surface area of the nanomaterial. To tackle this issue, we used a cationic hydrophilic polymer, PEI as the capping agent; PEI not only improves ZnO dispersion in biological fluid but also provides a layer of positive charge over the nanoparticle surface. Different surface modifications on the gold nanoparticle resulted in diverse response on the structure and stability of the protein.[42,59] However, there is no systematic investigation on the response of differentially substituted ZnO nanoparticles with protein. Here we explore the consequence of PEI surface modification on ZnO NP on the interaction with BSA and the resulting effect on the protein structure.

Thermodynamics of Interaction. The adsorption of proteins over the nanomaterials' surface is a complex process and depends upon several factors such as the nature of the protein, physiochemical properties of the surface of the nanomaterials, and the binding force involved in the interaction that subsequently affects the structure and activity of the protein.[29,60,61] The maintenance of the integrity of the protein structure on adsorption to nanoparticle is desirable to avoid any adverse effects on cellular processes.[62] Isothermal titration caloriemetry (ITC) is the most direct and reliable technique to study protein adsorption over the nanoparticle.[63] Previously Rotello and his co-workers used ITC extensively to investigate protein−gold nanoparticle (GNP) interaction, which they found to be largely dependent on surface charge and hydrophobicity of the capping agent.[64] The authors also highlighted the importance of electrostatic interaction on GNP−protein complex formation.[64] The same technique was used here to decipher the nature of the interaction between different surface-functionalized ZnO and BSA. The thermodynamic parameters given by ITC reveal that both enthalpy and entropy contribute toward the ZnO−BSA assembly process (Figures 2 and S5 and Table 1), as opposed to ZnO-PEI−BSA interaction, where binding is essentially driven by enthalpy. According to Ross and Subramanian, enthalpic contribution in any protein−ligand interaction is caused by electrostatic interaction, whereas entropic contribution is an outcome of hydrophobic interaction.[49] The hydrophobic counterpart in the ZnO−BSA interaction arises from the hydrophobic nature of the ZnO NP itself,[65] and the electrostatic contribution is an outcome of a small positive charge that the NP surface bears (isoelectric point of ZnO ~9.4)[31] at physiological pH due to the adsorption of a H^+ ion. Once the surface of ZnO was

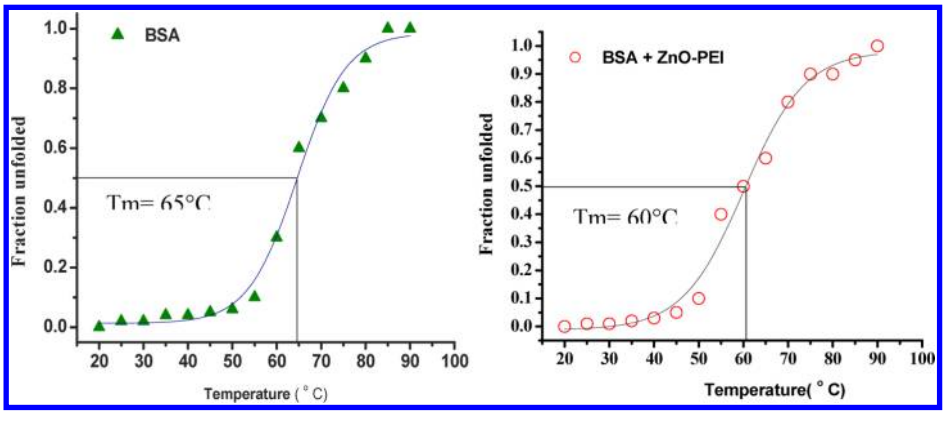

Figure 6. Thermal unfolding of BSA alone and in the presence of ZnO-PEI. Data were fitted to a sigmoidal equation.

dx.doi.org/10.1021/la3007603 | Langmuir 2012, 28, 11142−11152

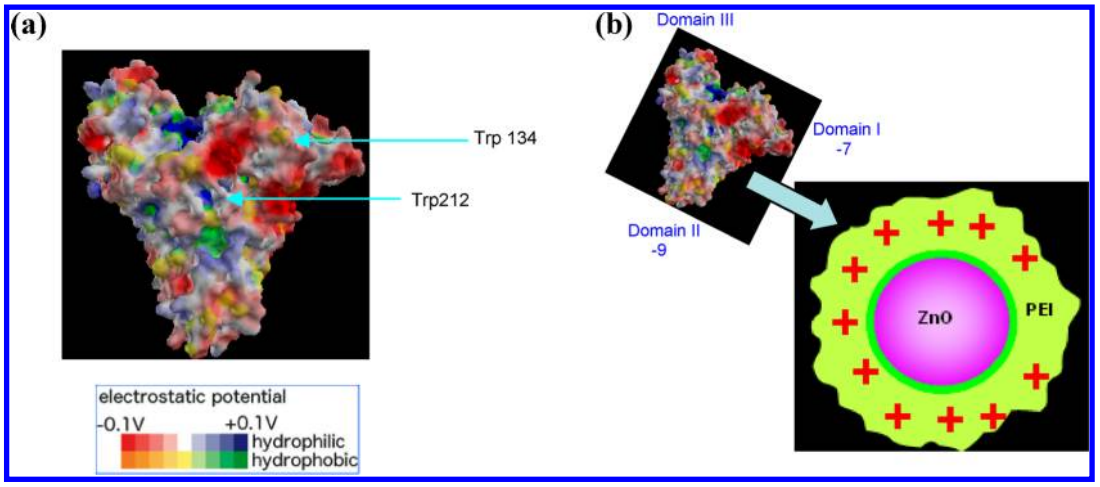

Figure 7. (a) eF-site generated electrostatic potential map of BSA. (b) Cartoon representation of ZnO-PEI approaching BSA (made using eF-site).

modified with the cationic polymer PEI, the surface charge of NP is drastically shifted to higher positive value, which leads to selective electrostatic interaction with the protein. Xiao et al. in a separate investigation involving HSA-CdSe/ZnS complex formation also observed the dominant role of electrostatic interaction.[66]

The size of ZnO-PEI is 20 nm, whereas that of ZnO NP is 7 nm.[31] However, we did not observe any significant change in effective surface coverage by the protein on PEI capping (7.8% versus 7.2%, Table S3), although the association constant between two components increases by almost 3-fold (Table 1). The increased binding constant indicates the selectivity of PEI toward an acidic protein, such as albumin. The results indicate that a rather hydrophobic nanoparticle (ZnO), on specific (PEI) capping, can be made to have predominantly electrostatic interaction with BSA.

Putative Binding Site of ZnO-PEI and ZnO NP on BSA. BSA is a transport protein; it possesses numerous sites for ligand binding. Depending on the nature of the ligand, the binding site on BSA varies. The heart-shaped BSA has three domains, domain I (residues 1−195), II (residues 196−383), III (residues 384−583).[36] Domain I (−7) and domain II (−9) are negatively charged, whereas domain III is neutral at physiological pH (Figure 7 and Table S4). The discrepancy in charge distribution over different domains originally comes from the differential location of surface-exposed acidic and basic residues and has been noted earlier.[67] PEI is a cationic polymer rich in amino group and prefers electrostatic binding with protein. In BSA, the electrostatic binding occurs via domains I and II, as is the case with ZnO-PEI, enumerated in the previous section. BSA adsorption over solid surface generally involves two specialized modes, (i) side-on and (ii) end-on. Side-on is the preferred mode of BSA adsorption over end-on as it covers the greater surface area of the protein (49.5 nm^2 versus 30.3 nm^2).[68] Evidence also comes from fluorescence quenching result which shows that ZnO-PEI binds BSA at the surface close to Trp134, which can happen if the protein is adsorbed over the NP in the side-on mode (Figure 7b). An earlier study also reported that side-on overlapping is the normally preferred mode of BSA adsorption over the positively charged (Al_2O_3) nanoparticles.[68] Although ITC suggests the involvement of electrostatic interactions, as also supported by earlier studies, it may be mentioned that the fluorescence quenching cannot unequivocally be attributed to the binding near Trp134—it is possible that the small changes in the secondary structure that has been observed on ZnO-PEI binding may lead to Trp212 being exposed to either the solution or the NP.

It has been reported that colloidal ZnO quenches tryptophan fluorescence in BSA;[69,70] however, the exact location of ZnO within BSA was not ascertained. Our ITC data (Table 1 and Figure S5), indicative of substantial entropic contribution to binding, suggest that ZnO uses the hydrophobic surface for attachment. As mentioned earlier, BSA contains two tryptophan residues of which Trp134 is surrounded by acidic residues and Trp212 is located near the vicinity of a hydrophobic cavity (Sudlow's site I). The binding of colloidal ZnO near Trp212 could be responsible for the fluorescence quenching observed earlier, although a minor involvement of Trp134 in the quenching process cannot be ruled out considering the size of the nanoparticle (7 nm) and protein (~5.5 nm). A further confirmation of binding of the ZnO NP at the Sudlow's site I comes from the competitive binding experiment using a marker drug, warfarin (Figure S6).

Structure and Stability of BSA on Binding to Uncapped and PEI-Capped ZnO. There are several reports on colloidal ZnO−BSA binding with a binding constant of ~10^4.[69,70] The binding is achieved by simultaneous participation of both electrostatic and hydrophobic forces in the interaction process (Table 4). It is believed that hydrophobic interaction could have a deleterious effect on protein structure and function[71] as new hydrophobic interaction between the protein and nanoparticle comes at the expense of old intramolecular hydrophobic contacts in the proteins. It has been shown that the carbon nanotube (one form of hydrophobic nanoparticle) can plug inside the hydrophobic cores of protein to form stable complexes leading to disruption of protein function by blocking the active site.[72] Likewise, the interaction with colloidal ZnO also leads to structural deformation in BSA,[69] especially at higher concentrations of NP (~10% loss in helical structure) (Table 4). This is also manifested by alteration in thermal and chemical stability of the protein (unpublished data). In contrast, ZnO-PEI has lesser effects on protein structure and stability as it involves electrostatic interaction. Similar result was found in case of CNT-PEI-albumin interaction,[73] which also supports the general belief that electrostatic interaction with NPs is associated with a lesser extent of modification in the native structure.[74]

dx.doi.org/10.1021/la3007603 | Langmuir 2012, 28, 11142−11152

Table 4. Effect of ZnO NP and ZnO-PEI on the Structure, Function, and Stability of BSA

feature/parameter	ZnO NP	ZnO-PEI
binding constant	$(2.5-5.8) \times 10^4$ [a,69,70]	$7.94 (\pm 3) \times 10^4$
binding thermodynamics	both enthalpy- and entropy-driven[69]	primarily enthalpy-driven
binding stoichiometry (protein:NP)	1[a,69,70]	0.3
interaction type	electrostatic[64] + hydrophobic	primarily electrostatic
helical structure alteration	10% loss[69]	marginal loss
fluorescence quenching and lifetime	static type of quenching, with no change in lifetime[69]	static quenching
possible binding site	Sudlow's site I, near Trp212	binds at surface
change in activity	9%	5%
chemical; thermal stability (melting temperature, T_m) in the presence of NP	little destabilized; 10 °C loss in T_m[b]	negligible effect on stability; 5 °C loss in T_m
effective surface coverage	7.8%	7.2%

[a]Based on this work. Reference numbers for earlier work are provided. [b]Our unpublished data.

CONCLUSIONS

In this paper, we have reported how PEI modification over ZnO affects the structure, function, and stability of BSA as compared to uncapped ZnO. There are a few salient features. (i) The binding between ZnO-PEI and BSA occurs via electrostatic interactions, in contrary to ZnO where hydrophobic forces have an important role. Further, the binding constant between ZnO and BSA increases by ∼3 times on PEI capping. (ii) ZnO-PEI binds BSA on its surface involving the surface-exposed Trp134. In comparison, the uncapped ZnO binds at the hydrophobic Sudlow's site I and quenches fluorescence, most likely form Trp212 (Table 4). (iii) ZnO-PEI binding has less deleterious effect on the structure, stability, and activity (Figure S7) of the protein in contrast to that of ZnO. The structural alteration due to ZnO NP supports the idea that hydrophobic interaction is associated with protein structural deformation.[71,72] In summary, we have demonstrated that the functionality of ZnO could easily be tailored by PEI to make it more hydrophilic, allowing favorable interaction with serum albumin. This work demonstrates the importance of surface coating and the stability it confers to the interaction process. Protein-mediated nanoparticle internalization is at present a hotspot of research. We believe that the present investigation on the molecular interactions involving derivatized ZnO nanoparticles and BSA would establish a better understanding of the adsorption and internalization of PEI-functionalized nanoparticles in vivo.

ASSOCIATED CONTENT

Supporting Information

Additional experimental details are given in seven figures and four tables. Figure S1 describes a schematic synthesis route of ZnO-PEI preparation. Figure S2 shows the UV−visible and FTIR characteristic spectra of ZnO-PEI. Figure S3 provides the details of electron microscopic measurements of ZnO-PEI. Figure S4 shows the far-UV CD spectra and helix-to-coil transition of BSA in the presence of varying concentration of ZnO NP. Figure S5 provides the ITC data of BSA−ZnO interaction. Figure S6 displays the competition assay between warfarin and ZnO NP for binding to BSA. Figure S7 describes the relative esterase activity of BSA in the absence and presence of NPs. Table S1 provides the calculation to evaluate the NP/PEI ratio in ZnO-PEI. Table S2 presents the secondary structural elements of BSA in the presence of varying concentration ZnO-PEI. Table S3 shows the surface coverage of BSA over ZnO NP and ZnO-PEI. Table S4 depicts domain-wise charge distribution of BSA. This material is available free of charge via the Internet at http://pubs.acs.org.

AUTHOR INFORMATION

Corresponding Author

*E-mail: singhsp@mail.nplindia.ernet.in, pinak@boseinst.ernet.in.

Author Contributions

‖These authors contributed equally.

Notes

The authors declare no competing financial interest.

ACKNOWLEDGMENTS

P.C. is supported by the JC Bose National Fellowship. S.C. and P.J. are thankful to the Council of Scientific and Industrial Research, India, for research fellowships. S.P.S. acknowledges the support from the Director, National Physical Laboratory, New Delhi and IFN start up Grant OIA-0701525 at the University of Puerto Rico, Mayaguez.

REFERENCES

(1) Ferrari, M. *Nat. Rev. Cancer* **2005**, *5*, 161−171.
(2) Gao, X.; Cui, Y.; Levenson, M.; Chung, L. W. K.; Nie, S. *Nat. Biotechnol.* **2004**, *22*, 969−976.
(3) De, M.; Ghosh, P. S.; Rotello, V. M. *Adv. Mater.* **2008**, *20*, 4225−4241.
(4) Saito, N.; Haneda, H.; Sekiguchi, N.; Ohashi, I.; Sekiguchi, K.; Kaumoto, K. *Adv. Mater.* **2002**, *14*, 418−421.
(5) Yang, P. D.; Yan, H. Q.; Mao, S.; Russo, R.; Johnson, J.; Saykally, R.; Morris, N.; Pham, J.; He, R. R.; Choi, H. J. *Adv. Funct. Mater.* **2002**, *12*, 323−331.
(6) Bai, X. D.; Wang, E. G.; Gao, P. X.; Wang, Z. L. *Nano Lett.* **2003**, *3*, 1147−1150.
(7) Yang, M.; Wang, D.; Lin, Y.; Li, Z.; Zhang, Q. *Mater. Chem. Phys.* **2004**, *88*, 333−338.
(8) Son, J. Y.; Lim, S. J.; Cho, J. H.; Seong, W. K.; Kim, H. *Appl. Phys. Lett.* **2008**, *93*, 053109.
(9) Huang, M. H.; Mao, S.; Feick, H.; Yan, H. Q.; Wu, Y. Y.; Kind, H.; Weber, E.; Russo, R.; Yang, P. D. *Science* **2001**, *292*, 1897−1899.
(10) Wang, X.; Kong, X.; Yu, Y.; Zhang, H. *J. Phys. Chem. C* **2007**, *111*, 3836−3841.
(11) Wu, Y. L.; Lim, C. S.; Fu, S.; Tok, A. I. K.; Lau, H. M.; Boey, F. Y. C.; Zeng, X. T. *Nanotechnology* **2007**, *18*, 215604.
(12) Rasmussen, J. W.; Martinez, E.; Louka, P.; Wingett, D. G. *Expert Opin. Drug Delivery* **2010**, *7*, 1063−1077.
(13) Xiong, H. M.; Xu, Y.; Ren, Q. G.; Xia, Y. Y. *J. Am. Chem. Soc.* **2008**, *130*, 7522−7523.
(14) Bruchez, M., Jr.; Moronne, M.; Gin, P.; Weiss, S.; Alivisatos, A. P. *Science* **1998**, *281*, 2013−2016.
(15) Fu, Y. S.; Du, X. W.; Kulinich, S. A.; Qiu, J. S.; Qin, W. J.; Li, R.; Sun, J.; Liu, J. *J. Am. Chem. Soc.* **2007**, *129*, 16029−16033.
(16) Joshi, P.; Ansari, Z. A.; Singh, S. P.; Shanker, V. *Adv. Sci. Lett.* **2009**, *2*, 360−363.
(17) Boussif, O.; Zanta, M. A.; Behr, J. P. *Gene Ther.* **1996**, *3*, 1074−1080.
(18) Dunlap, D. D.; Maggi, A.; Soria, M. R.; Monaco, L. *Nucleic Acids Res.* **1997**, *25*, 3095−3101.

(19) Hashemil, M.; Parhiz1, B. H.; Hatefi, A.; Ramezani, M. *Cancer Gene Ther.* **2011**, *18*, 12−19.
(20) Neville, F.; Broderick, M. J. F.; Gibson, T.; Millner, P. A. *Langmuir* **2011**, *27*, 279−285.
(21) Sun, S. K.; Wang, H. F.; Yan, X. P. *Chem. Commun.* **2011**, *47*, 3817−3819.
(22) Beyth, N.; Houri-Haddad, Y.; Baraness-Hadar, L.; Yudovin-Farber, I.; Domb, A. J.; Weiss, E. I. *Biomaterial* **2008**, *29*, 4157−4163.
(23) Beyth, N; Yudovin-Farber, I.; Perez-Davidi, M.; Domb, A. J.; Weiss, E. I. *Proc. Natl. Acad. Sci. U.S.A.* **2010**, *107*, 22038−22043.
(24) Lee, H. J.; Lee, S. G.; Oh, E. J.; Chung, H. Y.; Han, S. I.; Kim, E. J.; Seo, S. Y.; Ghim, H. D.; Yeum, J. H.; Choi, J. H. *Colloids Surf., B* **2011**, *88*, 505−511.
(25) Xia, T.; Kovochich, M.; Liong, M.; Meng, H.; Kabehie, S.; George, S.; Zink, J. I.; Nel, A. E. *ACS Nano* **2009**, *3*, 3273−3286.
(26) Beyerle, A.; Long, A. S.; White, P. A.; Kissel, T.; Stoeger, T. *Mol. Pharmaceutics* **2011**, *8*, 976−981.
(27) Lynch, I.; Dawson, K. A. *Nano Today* **2008**, *3*, 40−47.
(28) Vertegel, A. A.; Siegel, R. W.; Dordick, J. S. *Langmuir* **2004**, *20*, 6800−6807.
(29) De, M.; You, C. C.; Srivastava, S.; Rotello, V. M. *J. Am. Chem. Soc.* **2007**, *129*, 10747−10753.
(30) Vannoy, C. H.; Leblanc, R. M. *J. Phys. Chem. B* **2010**, *114*, 10881−10888.
(31) Chakraborti, S.; Chatterjee, T.; Joshi, P.; Poddar, A.; Bhattacharyya, B.; Singh, S. P.; Gupta, V.; Chakrabarti, P. *Langmuir* **2010**, *26*, 3506−3513.
(32) Joshi, P.; Chakraborty, S.; Dey, S.; Shanker, V.; Ansari, Z. A.; Singh, S. P.; Chakrabarti, P. *J. Colloid Interface Sci.* **2011**, *355*, 402−409.
(33) Chatterjee, T.; Chakraborti, S.; Joshi, P.; Singh, S. P.; Gupta, V.; Chakrabarti, P. *FEBS J.* **2010**, *277*, 4184−4194.
(34) Uversky, V. N.; Narizhneva, N. V.; Ivanova, T. V.; Tomashevskis, A. Y. *Biochemistry* **1997**, *36*, 13638−13645.
(35) Jisha, V. S.; Arun, K. T.; Hariharan, M.; Ramaiah, D. *J. Am. Chem. Soc.* **2006**, *128*, 6024−6025.
(36) He, X. M.; Carter, D. C. *Nature* **1992**, *358*, 209−215.
(37) Kim, S. H.; Jeong, J. H.; Chun, K. W.; Park, G. *Langmuir* **2005**, *21*, 8852−8857.
(38) Chithrani, B. D.; Ghazani, A. A.; Chan, W.C. W. *Nano Lett.* **2006**, *6*, 662−668.
(39) Carrabino, S.; Gioia, S. D.; Copreni, E.; Conese, M. *J. Gene Med.* **2005**, *7*, 1555−1564.
(40) Xu, Y.; Mazzawi, M.; Chen, K.; Sun, L.; Dubin, P. L. *Biomacromolecules* **2011**, *12*, 1512−1522.
(41) Velazquez-Campoy, A.; Leavitt, S. A.; Freire, E. *Methods Mol. Biol.* **2004**, *261*, 35−54.
(42) Chakraborty, S.; Joshi, P.; Shanker, V.; Ansari, Z. A.; Singh, S. P.; Chakrabarti, P. *Langmuir* **2011**, *27*, 7722−7731.
(43) Lakowicz, J. R. *Principles of Fluorescence Spectroscopy*, 3rd ed.; Springer: New York, 2006.
(44) Mandal, A. K.; Samaddar, S.; Banerjee, R.; Lahiri, S.; Bhattacharyya, A.; Roy, S. *J. Biol. Chem.* **2003**, *278*, 36077−36084.
(45) Suji, G.; Khedkar, S. A.; Singh, S. K.; Kishore, N.; Coutinho, E. C.; Bhor, V. M.; Sivakami, S. *Protein J.* **2008**, *27*, 205−214.
(46) Dolinsky, T. J.; Czodrowski, P.; Li, H.; Nielsen, J. E.; Jensen, J. H.; Klebe, G.; Baker, N. A. *Nucleic Acids Res.* **2007**, *35*, W522−W525.
(47) Dolinsky, T. J.; Nielsen, J. E.; McCammon, J. A.; Baker, N. A. *Nucleic Acids Res.* **2004**, *32*, W665−W667.
(48) Baker, N. A.; Sept, D.; Joseph, S.; Holst, M. J.; McCammon, J. A. *Proc. Natl. Acad. Sci. U.S.A.* **2001**, *98*, 10037−10041.
(49) Ross, P. D.; Subramanian, S. *Biochemistry* **1981**, *20*, 3096−3102.
(50) Pan, T.; Xiao, Z. D.; Huang, P. M. *J. Lumin.* **2009**, *129*, 741−745.
(51) Weert, M; van de Stella, L. *J. Mol. Struct.* **2011**, *998*, 144−150.
(52) Laera, S.; Ceccone, G.; Rossi, F.; Gilliland, D.; Hussain, R.; Siligardi, G.; Calzolai, L. *Nano Lett.* **2011**, *11*, 4480−4484.
(53) Tam, M. A.; Hamad-Schifferli, K. *Langmuir* **2005**, *21*, 12080−12084.
(54) Cedervall, T.; Lynch, I.; Lindman, S.; Berggård, T.; Thulin, E.; Nilsson, H.; Dawson, K. A.; Linse, S. *Proc. Natl. Acad. Sci. U.S.A.* **2007**, *104*, 2050−2055.
(55) Wu, X.; Narsimhan, G. *Langmuir* **2008**, *24*, 4989−4998.
(56) Wu, X; Narsimhan, G. *Biochim. Biophys. Acta* **2008**, *1784*, 1694−1701.
(57) Lacerda, S. H. D. P.; Park, J. J.; Meuse, C.; Pristinski, D.; Becker, M. L.; Karim, A.; Douglas, J. F. *ACS Nano* **2010**, *4*, 365−379.
(58) Teichroeb, J. H.; Forresta, J. A.; Jones, L. W. *Eur. Phys. J. E* **2008**, *26*, 411−415.
(59) Gagner, J. E.; Lopez, M. D.; Dordick, J. S.; Siegel, R. W. *Biomaterial* **2011**, *32*, 7241−7252.
(60) Shang, W.; Nuffer, J. H.; Dordick, J. S.; Siegel, R. W. *Nano Lett.* **2007**, *7*, 1991−1995.
(61) Fischer, N. O.; McIntosh, C. M.; Simard, J. M.; Rotello, V. M. *Proc. Natl. Acad. Sci. U.S.A.* **2002**, *99*, 5018−5023.
(62) Sperling, R. A.; Parak, W. J. *Philos. Trans. R. Soc., A* **2010**, *368*, 1333−1338.
(63) Lindman, S.; Lynch, I.; Thulin, E.; Nilsson, H.; Dawson, K. A.; Linse, S. *Nano Lett.* **2007**, *7*, 914−920.
(64) You, C. C.; De, M.; Han, G.; Rotello, V. M. *J. Am. Chem. Soc.* **2005**, *127*, 12873−12881.
(65) Tso, C. P.; Zhung, J. M.; Shih, Y. H.; Tseng, Y. M.; Wu, S. C.; Doong, Y. A. *Water Sci. Technol.* **2010**, *61.1*, 127−133.
(66) Xiao, Q.; Huang, S.; Qi, Z. D.; Zhou, B.; He, Z. K.; Liu, Y. *Biochim. Biophys. Acta* **2008**, *1784*, 1020−1027.
(67) Peters, T., Jr. *Adv. Protein Chem.* **1985**, *37*, 161.
(68) Rezwan, K.; Meier, P. L.; Rezwan, M.; Voros, J.; Textor, M.; Guckler, G. J. *Langmuir* **2004**, *20*, 10055−10061.
(69) Bardhan, M.; Mandal, G.; Ganguly, T. *J. Appl. Phys.* **2009**, *106*, 034701−034705.
(70) Kathirvan, A.; Paramaguru, G.; Renganathan, R. *J. Mol. Struct.* **2009**, *934*, 129−137.
(71) Mahamoudi, M.; Lynch, I.; Ejtehadi, M. J.; Monopoli, M. P.; Bombelli, F. B.; Laurent, S. *Chem. Rev.* **2011**, *111*, 5610−5637.
(72) Zuo, G.; Huang, Q.; Wel, G.; Zhei, R.; Zhou, R.; Fang, H. *ACS Nano* **2011**, *4*, 7508−7514.
(73) Chen, M. L.; Chen, M. L.; Chen, X. W.; Wang, J. H. *Macromol. Biosci.* **2010**, *10*, 906−915.
(74) Larsericsdotter, H.; Oscarsson, S.; Buijs, J. *J. Colloid Interface Sci.* **2001**, *231*, 98−103.